Article

Not peer-reviewed version

Structural Studies of Monounsaturated and ω-3 Polyunsaturated Free Fatty Acids in Solution with the Combined Use of NMR and DFT calculations - Comparison with the Liquid State

Ioannis P. Gerothanassis *, Michael G. Siskos, Georgios Papamokos *, Themistoklis Venianakis

Posted Date: 25 July 2023

doi: 10.20944/preprints202307.1662.v1

Keywords: 1D 1H NOE; 1H chemical shift; ALA; EPA; DHA; DFT

Review

Structural Studies of Monounsaturated and ω-3 Polyunsaturated Free Fatty Acids in Solution with the Combined Use of NMR and DFT Calculations - Comparison with the Liquid State

Themistoklis Venianakis, Michael Siskos, George Papamokos * and Ioannis P. Gerothanassis *

Section of Organic Chemistry and Biochemistry, Department of Chemistry, University of Ioannina, Ioannina, GR, 45110, Greece

* Correspondence: gpapamokos@seas.harvard.edu (G.P.); igeroth@uoi.gr (I.P.G.)

Abstract: Molecular structures, in chloroform and DMSO solution, of the monounsaturated free fatty acids (FFAs) caproleic acid (dec-9-enoic acid) and oleic acid (octadec-9-enoic acid) and the ω-3 FFAs α-linolenic acid (9Z,12Z,15Z)-octadeca-9,12,15-trienoic acid ALA), eicosapentanoic acid (5Z,8Z,11Z,14Z,17Z)-icosa-5,8,11,14,17-pentaenoic acid) and docosahexaenoic acid (4Z,7Z,10Z,13Z,16Z,19Z)-docosa-4,7,10,13,16,19-hexaenoic acid), are reported with the combined use of NMR and DFT calculations. Variable temperature and concentration chemical shifts of the COOH protons and transient 1D NOE experiments, in $CDCl_3$, demonstrate the major contribution of low molecular weight aggregates of dimerized fatty acids, through intermolecular hydrogen bond interactions of the carboxylic groups, with parallel and antiparallel interdigitated structures, even at the low concentration of 20 mM. For the dimeric DHA, a structural model of an intermolecular hydrogen bond through carboxylic groups and an intermolecular hydrogen bond between the carboxylic group of one molecule and the ω-3 double bond of a second molecule, is shown to play a role. In DMSO-d_6 solution the centro-symmetric hydrogen bond interactions are broken and the carboxylic groups form strong intermolecular hydrogen bond interactions with a discrete solvation molecule of DMSO. These solvation species form parallel and antiparallel interdigitated structures of low molecular weight. DFT structural models in $CHCl_3$ and DMSO, in agreement with the NMR data, are compared with the structures in the liquid state.

Keywords: 1D ^{1}H NOE; ^{1}H chemical shift; ALA; EPA; DHA; DFT

1. Introduction

Free fatty acids are carboxylic acids with long saturated or unsaturated aliphatic chains, with 4 to 28 carbon atoms, which are stored as triacylglycerol in adipose tissue. Saturated, mono- and polyunsaturated free fatty acids, in the form of glycerolipids and phospholipids, are the major lipid components of cell membranes [1–4]. Fatty acids play essential roles in maintaining the correct membrane fluidity and environment for membrane protein function. FFAs have, also, essential roles in the regulation of energy metabolism, inflammation, neurological and cardiovascular diseases [3–9]. Omega-3 FFAs are polyunsaturated fatty acids (PUFAs) which are characterized by the presence of a double bond, three atoms away from the terminal CH_3- group. Three of the most important ω-3 PUFAs for human diet and physiology are α-linolenic acid ((9Z,12Z,15Z)-octadeca-9,12,15-trienoic acid, ALA), eicosapentaenoic acid ((5Z,8Z,11Z,14Z,17Z)-icosa-5,8,11,14,17-pentaenoic acid, EPA) and docosahexaenoic acid ((4Z,7Z,10Z,13Z,16Z,19Z)-docosa-4,7,10,13,16,19-hexaenoic acid, DHA). ALA is widely distributed in plants, while DHA and EPA are found in algae and fish [1–3,10,11].

Structural and conformational properties of the unsaturated and the ω-3 FFAs have been investigated with the use of ^{1}H and ^{13}C NMR spectroscopy [10–14], molecular dynamics and molecular mechanics [15–17], and NMR and computational studies of mono- and polyunsaturated

 doi:10.20944/preprints202307.1662.v1

FFAs bound to human and bovine serum albumin and in competition with various drugs [18,19]. Combination of various physicochemical techniques and molecular dynamics simulations were reported to investigate membranes of 1-stearoyl(d_{35})-2-docosahexaenoyl-*sn*-glycero-3-phosphocholine and 1-stearoyl(d_{35})-2-docosapentaenoyl-*sn*-glycero-3-phosphocholine [20]. Law et al. [21] performed detailed DFT studies of a variety of conformations of ω-3 polyunsaturated free fatty acids. Translational motion, molecular conformation, and interdigitated hydrogen bonded aggregates in the liquid state of n-saturated and unsaturated free fatty acids were investigated with the use of ^{13}C NMR spin-lattice relaxation times, self-diffusion coefficients and X-ray diffraction at various temperatures [22,23]. Raman spectroscopy and differential scanning calorimetry [24] and 2D-NMR were used to investigate structures of polyunsaturated free fatty acids [25]. A quantum chemical study of the folding of EPA and DHA was reported by Bagheri et al. [26] and Veniannakis et al. [27,28] provided low energy structures of ω-3 fatty acids, in the liquid state, based on NMR and DFT calculations of ^1H NMR chemical shifts. Emphasis has been given on an atomistic structural model of DHA.

We report herein detailed structural studies of the monounsaturated caproleic and oleic acids, and the ω-3 polyunsaturated FFAs, α-linolenic acid, EPA, and DHA in chloroform and DMSO solution, with the combined use of NMR (variable concentration 1D transient NOEs and variable temperature NMR chemical shifts of the carboxylic groups) and DFT calculations. The results are compared with previous studies in the liquid state [27,28]. DFT atomistic structural models, in agreement with the NMR data, are critically evaluated.

2. Results and Discussion

2.1. Variable Temperature and Concentration ^1H NMR Chemical Shifts of Carboxylic Protons and 1D ^1H NMR Transient NOE in $CDCl_3$

The chemical shifts of the carboxylic protons, δ(COOH), and phenol OH group, δ(OH), are very informative criteria for the investigation of various types of hydrogen bond interactions [28–31]. δ(COOH) and δ(OH) are deshielded in the presence of hydrogen bond interactions and linear correlations between ^1H NMR chemical shifts and hydrogen bond distances have been reported [30,31]. Temperature has also a significant effect, thus, by increasing the temperature, the ^1H NMR chemical shifts are shielded due to breaking of hydrogen bond interactions (negative temperature coefficients, $\Delta\delta/\Delta T$). The ^1H NMR resonances of the COOH groups display broad signals at room temperature in $CDCl_3$. The broadening is mainly due to intermolecular proton exchange of the COOH group with the residual H_2O in $CDCl_3$ solution. The use of low concentrations ($c < 100$ mM) has a profound effect on proton exchange rate, which results in excessive line broadening and variable chemical shifts. The use of activated molecular shifts in the bottom of the NMR tube, but outside the active volume of the NMR coil, resulted in a significant reduction in the line widths which allowed the accurate determination of the chemical shifts and $\Delta\delta/\Delta T$ values.

δ(COOH) chemical shifts at 298 K, $\Delta\delta/\Delta T$ (ppb K^{-1}), and statistical analysis (coefficient of linear regression R^2 and intercept) of the data of Figure 1 are shown in Table 1. The temperature-dependent changes of the chemical shifts of the free fatty acids investigated are linear and the derived $\Delta\delta/\Delta T$ values, with $R^2 > 0.992$, cover a range of -42.74 to -29.52 ppb K^{-1}. These values are significantly larger, in absolute terms, than those obtained in the liquid state for caproleic acid, oleic acid, α-linolenic acid, EPA and DHA (-16.43 to -10.32 ppb K^{-1}) [28] (Table 1) and semi-fluorinated oleic, elaidic and stearic acids [32]. This shows that, by increasing the temperature, the intermolecular hydrogen bonds are more readily broken in $CDCl_3$ solution than those in the liquid state.

Numerous investigations of various carboxylic acids in CCl_4 and $CHCl_3$ were interpreted in terms of mixtures of cyclic and linear dimers, cyclic and linear trimers and monomers [33–39]. For long chain carboxylic acids, such as in FFAs, the formation of centro-symmetric hydrogen bond species through carboxylic groups appears to be the major structural mode. Thus, the single crystal X-ray structural analysis of linoleic acid, α-linolenic acid and arachidonic acid [40] showed the formation of centro-symmetric cyclic hydrogen bonds, which deviate from planarity by 26.7°, with

Preprints (www.preprints.org) | NOT PEER-REVIEWED | Posted: 25 July 2023 doi:10.20944/preprints202307.1662.v1

short O···O distances of 2.67 Å. Figure 1 and the data of Table 1 demonstrate that caproleic acid and oleic acid and the ω-3 ALA and EPA form intermolecular hydrogen bond interactions, since the chemical shifts of the carboxylic protons are strongly deshielded (11.17 to 10.39 ppm, at 298 K) (Table 1). In caproleic acid, oleic acid, ALA and EPA the hydrogen bond species through carboxylic groups, therefore, are the major components in $CDCl_3$ solution. This is in agreement with literature data [41] of the minor presence (1% to 3%) of the monomeric species in the liquid state for octanoic, nonanoic, decanoic and undecanoic acids in the temperature range of 280 K to 360 K.

The chemical shifts of the carboxylic groups of CA, OA, ALA, and EPA in $CDCl_3$ (Table 1) are slightly more shielded by 1.17 to 0.14 ppm, relative to those in the liquid state [28]. This can be attributed to the major role of the centro-symmetric cyclic dimers relative to contributions of other components of the equilibrium mixtures in both liquid state and $CDCl_3$ solution. Detailed dilution studies of caproleic acid in the range of 400 mM to 1 mM showed a very significant shielding in the concentration range below 15 mM due to increased contribution of the monomeric species. Thus, at 10 mM, the chemical shift of caproleic acid is ~ 8.6 ppm, while that of oleic acid, at 2 mM, is ~ 9.3 ppm. Further research in needed to determine the precise values of dimer-to-monomer dissociation constants, which apparently depend on the length of the side chain and the presence of multiple cis double bonds, as in the case of ω-3 fatty acids, which result in a significant 'kink' into the chain (see discussion below).

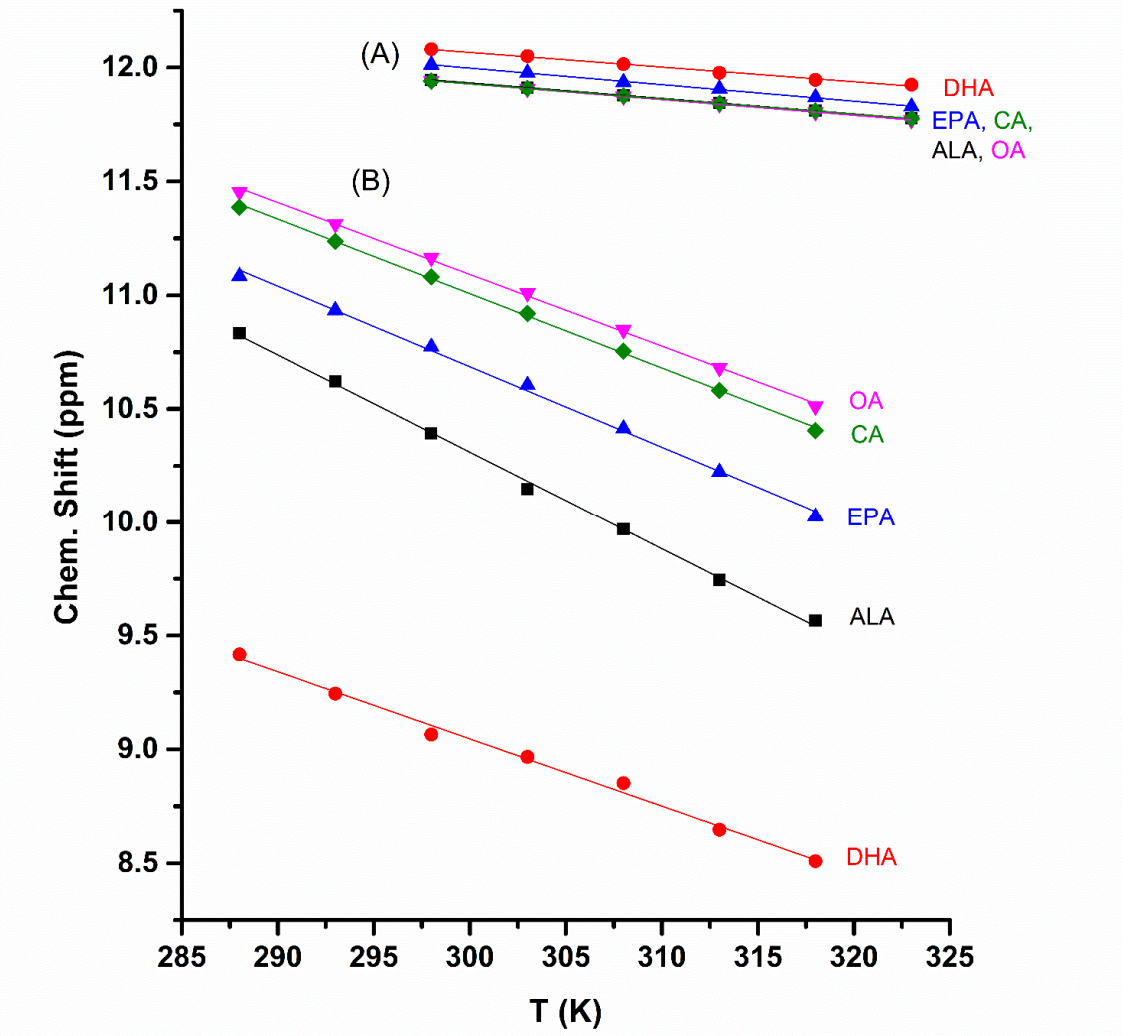

Figure 1. The temperature dependence of the COOH ^{1}H NMR chemical shifts of caproleic acid (CA), oleic acid (OA), ALA, EPA and DHA in DMSO-d_6, c = 20 mM (A) and $CDCl_3$, c = 40 mM (B).

Preprints (www.preprints.org) | NOT PEER-REVIEWED | Posted: 25 July 2023 doi:10.20944/preprints202307.1662.v1

Table 1. δ(COOH) chemical shifts at 298 K, Δδ/ΔT, and statistical analysis (R^2 and intercept) of the data of Figure 1 of δ(^{1}H) vs T(K) of the free fatty acids in $CDCl_3$ (c=40 mM), DMSO-d_6 (c=20 mM) and in the liquid state.

	$CDCl_3$				DMSO-d_6				Liquid state[a]			
FFA	**δ (ppm)**	**R^2**	**Δδ/ΔT (ppb K^{-1})**	**Inter.**	**δ (ppm)**	**R^2**	**Δδ/ΔT (ppb K^{-1})**	**Inter.**	**δ (ppm)**	**R^2**	**Δδ/ΔT (ppb K^{-1})**	**Inter.**
CA	11.08	0.999	-32.69	20.81	11.94	0.999	-6.62	13.92	12.25	0.999	-11.31	15.98
OA	11.17	0.999	-31.50	20.54	11.94	0.999	-6.88	13.99	12.13	0.998	-10.32	15.21
ALA	10.39	0.998	-42.74	23.13	11.95	0.999	-6.79	13.97	10.88	0.998	-13.06	14.76
EPA	10.77	0.997	-35.41	21.31	12.01	0.997	-7.27	14.18	10.91	0.999	-14.38	14.19
DHA	9.07	0.992	-29.52	17.90	12.08	0.993	-6.45	14.00	8.60	0.986	-16.43	13.51

[a] Ref. [28].

DHA is a particular case since the chemical shift of the carboxylic group is strongly shielded (δ = 9.07 ppm at 298 K). The chemical shift at 298 K is very similar to that in the liquid state (8.60 ppm) [28] and the Δδ/ΔT value (-29.52 ppb K^{-1}) is larger to that in the liquid state. It can, therefore, be concluded that for the dimeric DHA in $CDCl_3$, a structural mode of intermolecular hydrogen bonds through carboxylic groups and an intermolecular hydrogen bond between the carboxylic group of one molecule and the terminal double bond of the second molecule of DHA, plays a significant role, as in the case of the liquid state [28]. The OH···π hydrogen bond has been suggested to have significant structural roles in bioorganic chemistry [42,43] and biochemistry [44,45].

1D transient NOE experiments were performed for caproleic acid (CA), oleic acid (OA), α-linolenic acid (ALA), EPA, and DHA using various concentrations (100 mM, 50 mM, and 20 mM) in $CDCl_3$ and various mixing times, τ_m. The NOE grows during the period τ_m, starting from zero [33]. Figure 2 shows 1D NOE NMR spectra of oleic acid (OA) and α-linolenic acid (ALA) (concentration = 20 mM), using various τ_m values with selective excitation of the CH_3– group. Even for a short τ_m = 100 ms, there are weak NOE connectivities with the H2, H3 protons which are antiphase with respect to the irradiated CH_3– group. This is due to the formation of low molecular weight hydrogen-bonded species with τ_c values within the extreme narrowing condition ($\omega_o\tau_c << 1$) in the concentration range of 100 to 20 mM. By increasing τ_m, an approximately linear increase in the amplitude of the NOE signal intensities is observed which shows that the NOE is due to, through space, proximity of the CH_3– group and the $C\underline{H}_2$–$C\underline{H}_2$–COOH protons in the hydrogen bond species, rather than due to spin diffusion through the chain of the CH bonds.

Similar results were obtained with EPA (Figure 3A). The magnitude of all the NOE signal intensities of DHA, however, is significantly reduced relative to those of OA, ALA and EPA. This can be attributed to the formation of low molecular weight hydrogen-bonded aggregates in the range of minimum NOE signal intensities, i.e., $\omega_o\tau_c \sim 1$.

1D transient NOE NMR spectra of the caproleic acid (CA), with selective excitation of the α-CH_2 protons, is shown in the Supplementary Figure S1(A). As in the case of OA, ALA, EPA, and DHA the NOE connectivities are anti-phase with respect to the α-CH_2 group, due to the formation of low molecular weight hydrogen bond aggregates with τ_c values within the extreme narrowing condition ($\omega_o\tau_c << 1$). The magnitude of NOEs, however, with the terminal CH(9) = CH_2(10) protons was significantly less than those observed between α-CH_2 and the terminal CH_3- group of OA, ALA and EPA. This can be attributed to the minor formation of hydrogen bond interdigitated aggregates.

Preprints (www.preprints.org) | NOT PEER-REVIEWED | Posted: 25 July 2023 doi:10.20944/preprints202307.1662.v1

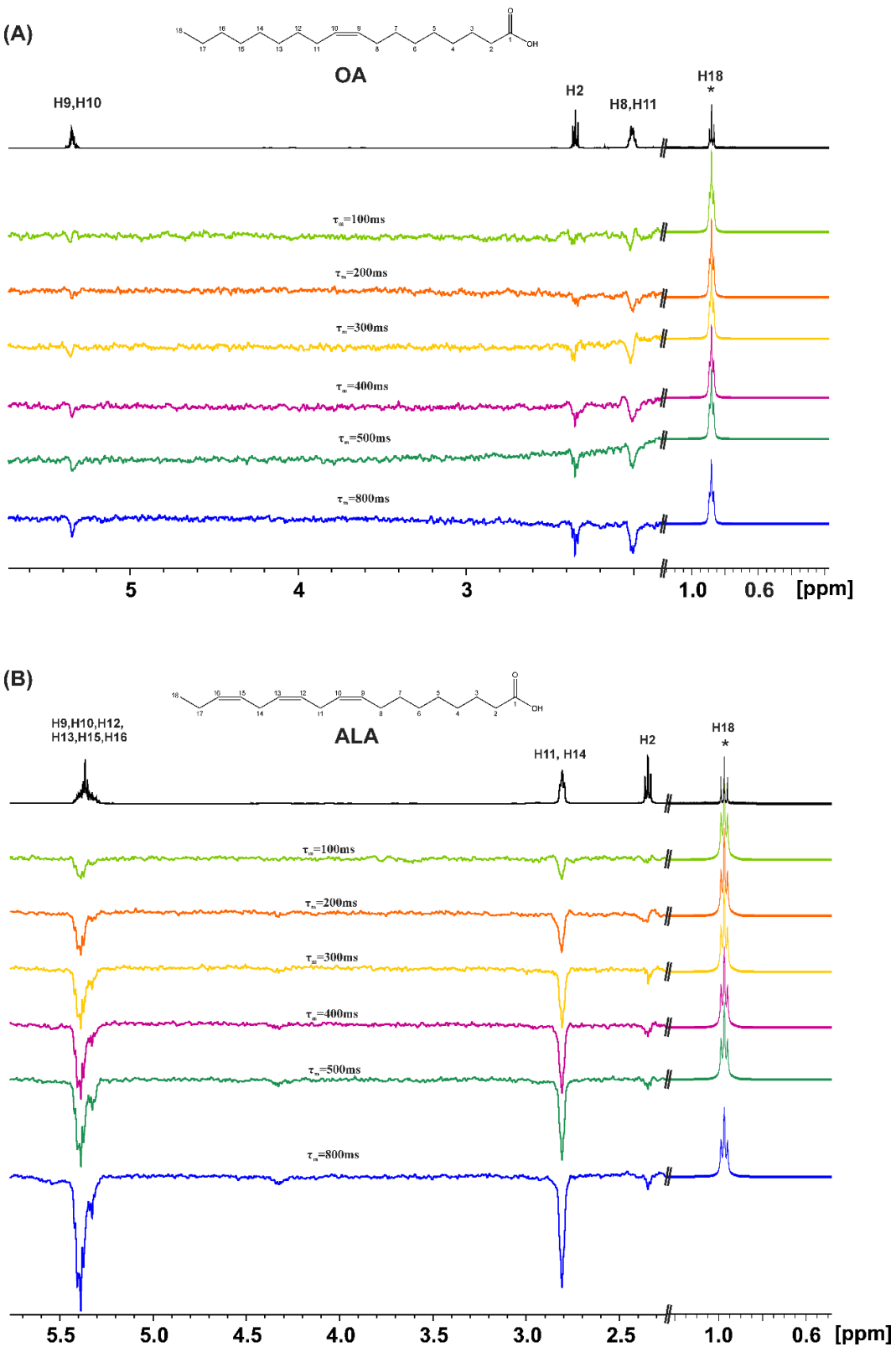

Figure 2. 1D transient NOE NMR spectra of: (A) oleic acid (OA) and (B) α-linolenic acid (ALA), concentration = 20 mM in $CDCl_3$ solution (number of scans=512, T=298K, T_{acq}=4.09s, relaxation delay=4s), using various τ_m values. The amplitude of the excited CH_3– group (denoted with the asterisk (*)), is reduced by a factor of 30, relative to the amplitude of the rest of the NOE signals.

Preprints (www.preprints.org) | NOT PEER-REVIEWED | Posted: 25 July 2023 doi:10.20944/preprints202307.1662.v1

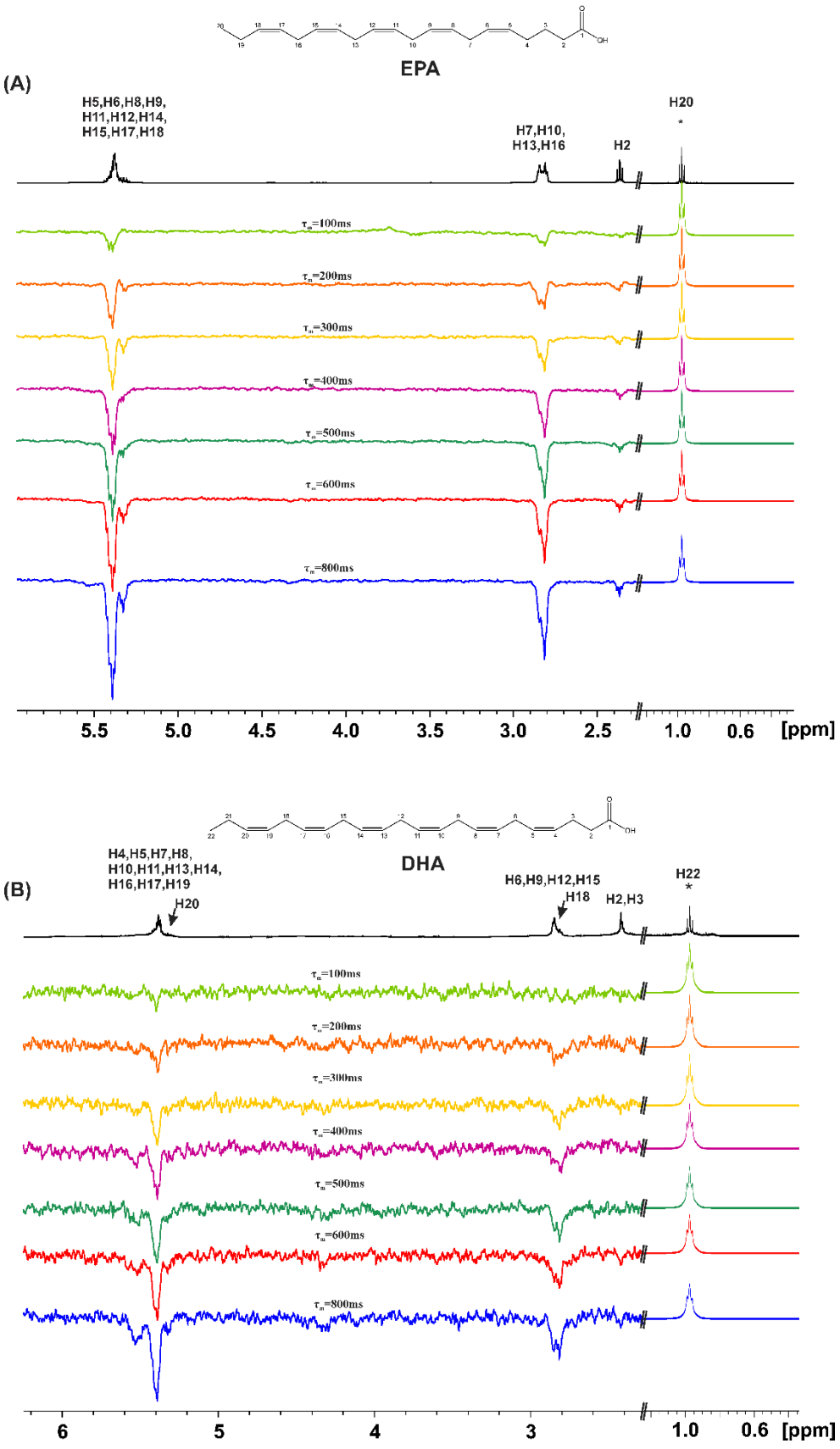

Figure 3. 1D transient NOE NMR spectra of: (A) EPA and (B) DHA, concentration = 20 mM in $CDCl_3$ at 298 K (number of scans = 512, T_{acq}=4.09s, relaxation delay=4s), using various τ_m values. The amplitude of the excited CH_3– group (denoted with the asterisk (*)), is reduced by a factor of 30, relative to the amplitude of the rest of the NOE signals.

 doi:10.20944/preprints202307.1662.v1

2.2. Variable Temperature ^{1}H NMR Chemical Shifts of Carboxylic Protons and 1D ^{1}H NMR Transient NOE in DMSO-d$_6$

Exchange broadening due to intermolecular proton exchange between COOH groups and residual H_2O, can be significantly eliminated in DMSO-d$_6$ due to its strong hydrogen bond and solvation ability. δ(COOH) and Δδ/ΔT values can, therefore, be determined accurately. The chemical shifts of the carboxylic protons, δ(COOH), in DMSO-d$_6$ solution (c = 20 mM) are very similar and appear in a very narrow chemical shift range for all the FFAs (11.94-12.08 ppm) and are more deshielded relative to those in $CDCl_3$ (Table 1 and Figure 1). This shows that the centro-symmetric cyclic dimers do not exist in DMSO-d$_6$ due to the strong hydrogen bond and solvation ability of the DMSO molecules. In DHA, the flip-flop process between the classical intermolecular centro-symmetric bonds through the carboxylic groups and an intermolecular hydrogen bond between the carboxylic group of one molecule and the terminal double bond of the second molecule of DHA is also eliminated in DMSO solution. Further confirmation was also obtained from the Δδ/ΔT values in DMSO-d$_6$ (-6.62 to -7.72 ppb K^{-1}) which are significantly smaller, in absolute terms, than those in $CDCl_3$. This demonstrates that the effect of increasing the temperature results in significantly less pronounced breaking of hydrogen bond interactions in DMSO-d$_6$, relative to those in $CDCl_3$ solution.

The great hydrogen bond and solvation ability of DMSO is clearly demonstrated from variable temperature experiments of an equimolar mixture of caproleic acid and DMSO-d$_6$. The chemical shift of the carboxylic proton at 298 K (δ = 11.90 ppm) and its temperature coefficient (Δδ/ΔT = -6.77 ppb K^{-1}) clearly show the elimination of the centro-symmetric cyclic dimers through the carboxylic groups.

1D transient NOE experiments were performed for the FFAs in DMSO-d$_6$ with concentration c=20mM. Figure 4 shows NOE NMR spectra of OA and ALA using various τ_m values with selective excitation of the terminal CH_3- group. Even for the relatively short τ_m = 100 ms, there are NOEs with the H2 and H3 protons which are antiphase with respect to the CH_3- group. This is due to the formation of low molecular weight hydrogen-bonded aggregates with τ_c values within the extreme narrowing condition ($\omega_o\tau_m \ll 1$). By increasing τ_m an increase in the amplitude of the NOE connectivities is observed which can be attributed to, through space, proximity of the CH_3–group and the $C\underline{H}_2$–$C\underline{H}_2$–COOH protons in the hydrogen bond species, rather than due to spin diffusion through the chain of the CH bonds.

Similar results were obtained with EPA and DHA (Figure 5). Selective excitation of the terminal CH_3- group results in anti-phase NOE connectivities with H2, H3, even for the relatively short mixing time τ_m = 100 ms. This demonstrates the proximity, through space, of the CH_3- group and the $C\underline{H}_2$–$C\underline{H}_2$–COOH protons in the low molecular weight hydrogen bond interdigitated aggregates, within the extreme narrowing condition ($\omega_o\tau_m \ll 1$).

1D transient NOE NMR spectra of caproleic acid (CA), using various τ_m values with selective excitation of α-CH_2 protons, are shown in the Supplementary Figure S1(B). The magnitude of the anti-phase NOEs, with the terminal CH(9)=CH_2(10) protons, was found to be significantly less than those observed between α-CH_2 and the terminal CH_3- groups of OA, ALA, EPA and DHA. This can be attributed to the minor formation of hydrogen bond interdigitated species.

Preprints (www.preprints.org) | NOT PEER-REVIEWED | Posted: 25 July 2023 doi:10.20944/preprints202307.1662.v1

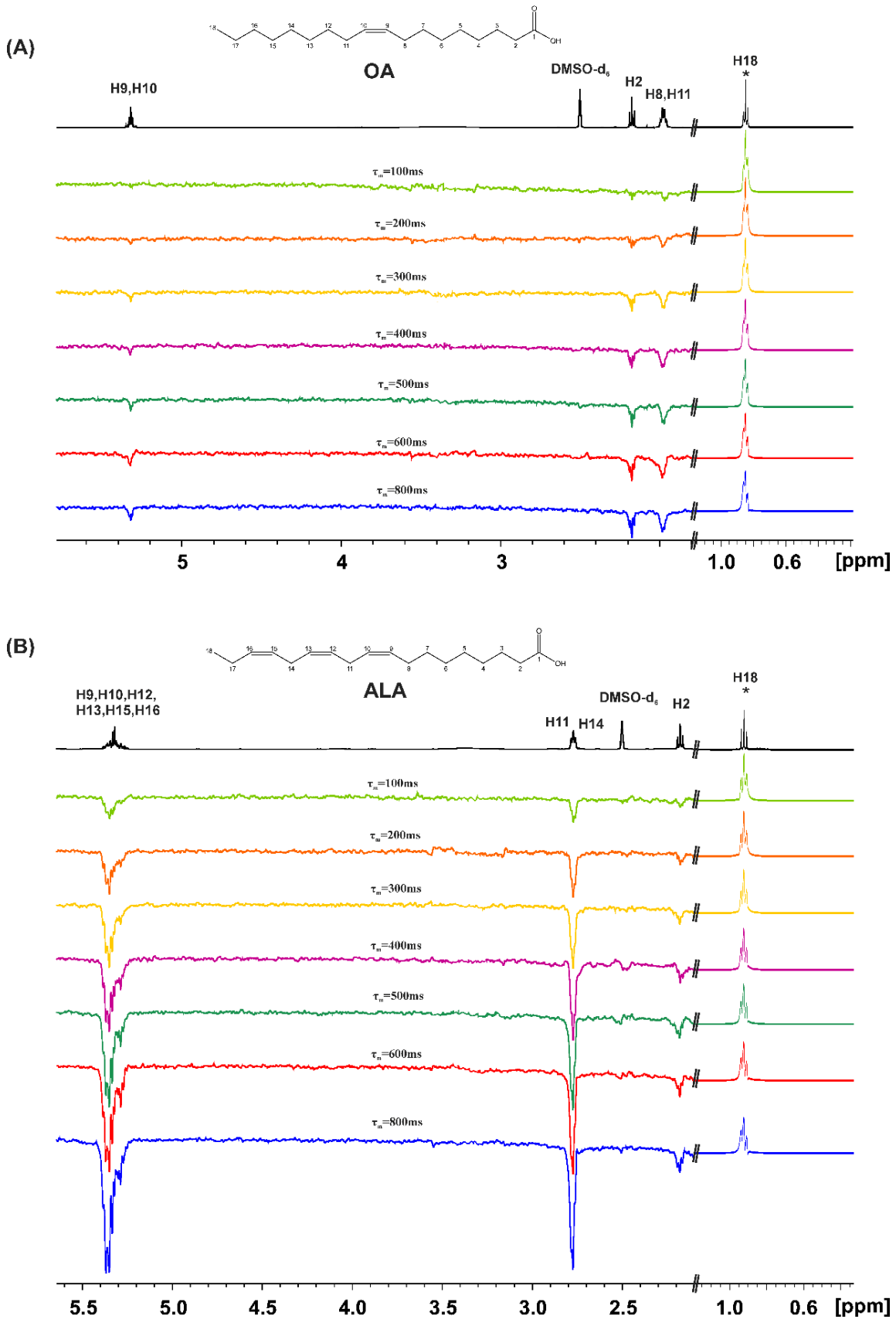

Figure 4. 1D transient NOE NMR spectra of: (A) oleic acid (OA) and (B) α-linolenic acid (ALA), concentration = 20 mM in DMSO-d$_6$ solution (number of scans=512, T=298K, T_{acq}=4.09s, relaxation delay=4s), using various τ_m values. The amplitude of the excited CH_3– group (denoted with the asterisk (*)), is reduced by a factor of 30, relative to the amplitude of the rest of the NOE signals.

Preprints (www.preprints.org) | NOT PEER-REVIEWED | Posted: 25 July 2023 doi:10.20944/preprints202307.1662.v1

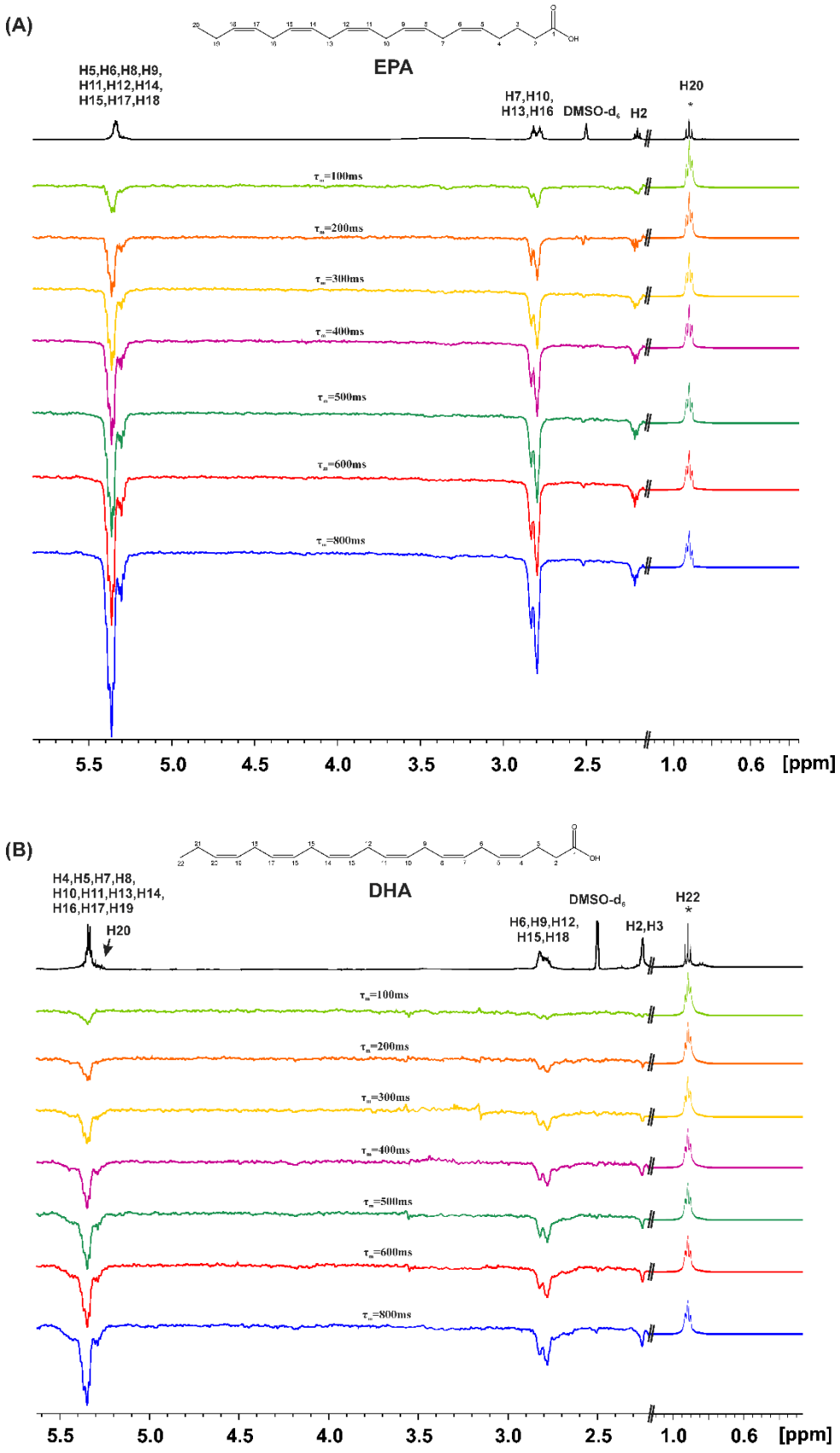

Figure 5. 1D transient NOE NMR spectra of: (A) EPA and (B) DHA, concentration = 20 mM in DMSO-d_6 at 298 K (number of scans = 512, T_{acq}=4.09s, relaxation delay=4s), using various τ_m values. The amplitude of the excited CH_3– group (denoted with the asterisk (*)), is reduced by a factor of 30, relative to the amplitude of the rest of the NOE signals.

Preprints (www.preprints.org) | NOT PEER-REVIEWED | Posted: 25 July 2023 doi:10.20944/preprints202307.1662.v1

2.3. DFT Calculations in $CHCl_3$ – Comparison with the Liquid State

Computational approaches have been proved very successful in elucidating structural and spectroscopic experimental data of free fatty acids in the liquid state [27,28]. Moreover, this approach can be used as a predictive tool in biotechnology for predesigned properties of functional free fatty acid aggregates by tuning their interatomic interactions in organic materials [46]. Based on the state of the FFA carboxylic proton, it can be determined if the FFA in the proper solution can be used as a transport or catalytic medium [47]. The present computations were designed to investigate possible inter- and intramolecular interactions that justify the experimental δ(COOH) and 1D NOE NMR results, presented above. Caproleic acid was investigated in the dimeric structure forming O–H···O=C centro-symmetric hydrogen bonds (Figure 6a), in the cyclic trimeric (Figure 6b) and linear trimeric (Figure 6c) structures in implicit solvation (IEFPCM-chloroform). In the centro-symmetric dimeric structure (Figure 6a), the dihedral angle defined by the four oxygen atoms of the carboxylic groups is only 0.8°, the (O)H···O(C) and O···O hydrogen bond distances are 1.66 and 2.65 Å, respectively, and the O–H···O bond angle is indicative of a nearly linear (178.0°) hydrogen bond interaction. These values can be compared with the O···O distance of 2.67 Å and deviation from planarity of 26.7° in the single crystal X-ray structure of linolenic acid, α-linolenic acid and arachidonic acid [40]. The experimental chemical shifts of caproleic acid (δ = 11.08 ppm at 298 K, Table 1) are rather indistinguishable on the basis of the structures of Figure 6a,b (13.6 ppm and 12.9/11.2/10/7 ppm, respectively, Table 2). In the linear aggregate structure Figure 6c, the presence of a carboxylic group which does not participate in hydrogen bond interactions (12.2/11.2/6.8 ppm), results in an average chemical shift of 10.4 ppm. A minor contribution of the structural model 6c, therefore, could account for the deviation of the experimental data from the computational data of the structures 6a and 6b. Moreover, the hydrophobic effect generated by the carbon chains in 6c, seems to play an antagonistic role with respect to the cyclic structure 6b.

Computations were also performed with the tetrameric caproleic acid, in a parallel orientation similar to the single crystal X-ray structures of free fatty acids [40] and in an antiparallel orientation, in agreement with the experimental weak NOE data of the through-space proximity of the α-CH_2 and the terminal CH(9)=CH_2(10) olefinic protons. Similar methodology was used for the interpretation of the NOEs observed in the liquid state for CA, OA, ALA, and EPA [28]. The calculated chemical shifts of the carboxylic proton for the tetrameric CA, in the parallel configuration vary between 14.3 and 13.0 ppm while in the antiparallel configuration between 13.8 and 13.2 ppm. The chemical shift difference of 1.3 ppm observed for the parallel arrangement can be attributed to the two interacting cyclic hydrogen bonds.

Table 2. Calculated δ(COOH) chemical shifts of the free fatty acids under study in implicit solvation (IEFPCM-chloroform).

FFA	Intermolecular interaction	δ(COO<u>H</u>) (ppm)
CA dimer	COO-H···O=COH	13.6
CA cyclic trimer	COO-H···O=COH	12.9/11.2/10.7
CA linear trimer	COO-H···O=COH	12.2/12.2
	COOH (free)	6.8
CA tetramer parallel	COO-H···O=COH	14.3, 14.0, 13.7, 13.0
CA tetramer antiparallel	COO-H···O=COH	13.8, 13.8, 13.8, 13.2

Preprints (www.preprints.org) | NOT PEER-REVIEWED | Posted: 25 July 2023 doi:10.20944/preprints202307.1662.v1

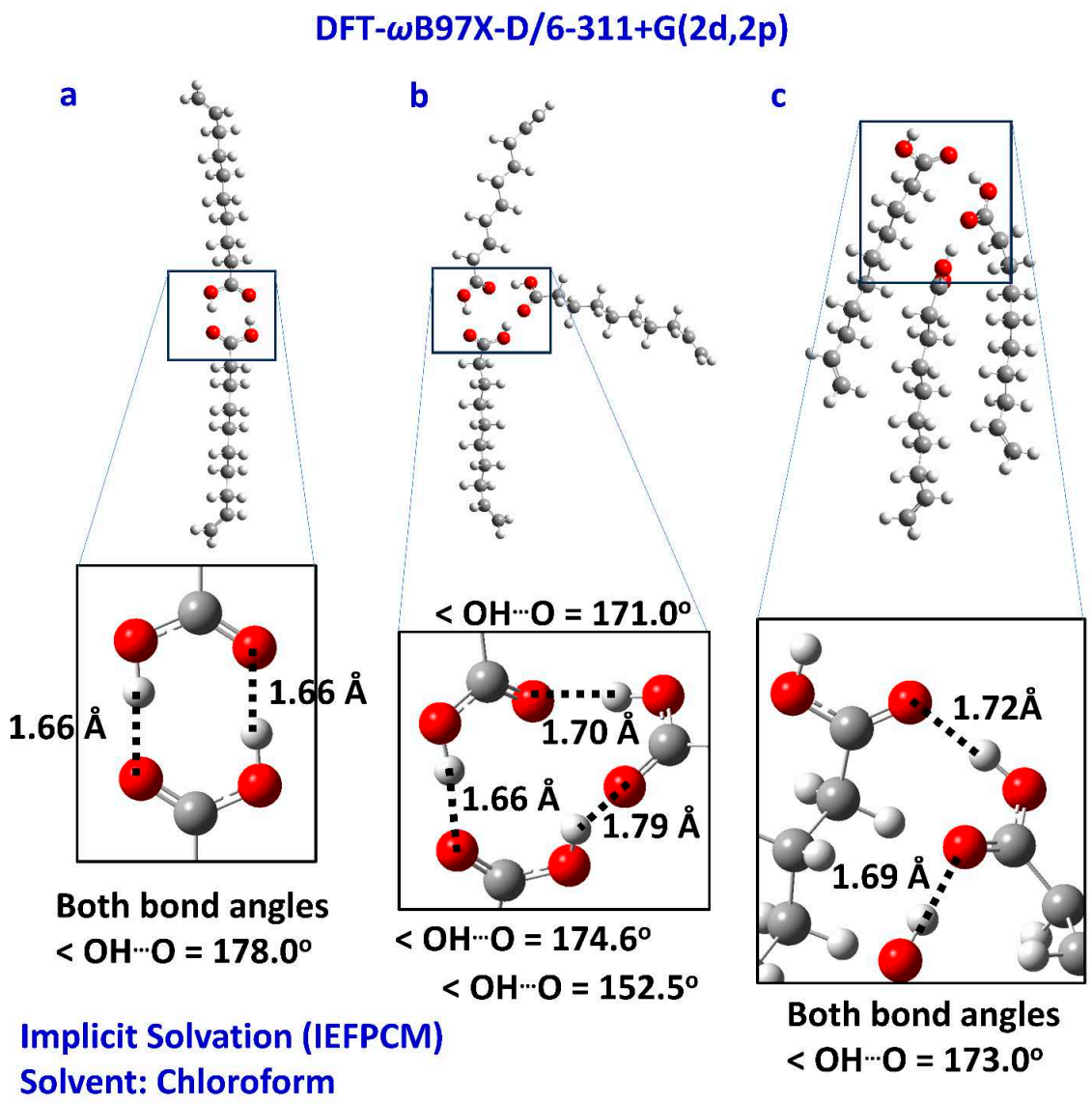

Figure 6. Optimized structures of caproleic acid: (a) dimeric structure forming OH···OC centro-symmetric hydrogen bonds. (b) Cyclic trimeric structure and (c) linear trimeric structure in implicit solvation (IEFPCM-chloroform).

2.4. DFT Calculations in DMSO

The DFT calculated ^{1}H NMR chemical shifts of the carboxylic protons with a discrete solvation molecule of DMSO were investigated in the case of a single molecule of CA, CA dimer with parallel and antiparallel arrangements (Figure 7 and Table 3). The representative molecular system is a caproleic acid molecule interacting with a DMSO molecule, explicitly present in the design, while the DMSO solvent is present implicitly (Figure 7a). To this interacting pair, another one, identical to the first, was added and oriented parallel and antiparallel to it (Figure 7b,c). These configurations were chosen to explore possible interactions between DMSO and the proton of the carboxylic group or the double bond of the caproleic acid and the proton of the carboxylic group. The results presented in Table 3 indicate that the orientations of Figure 7 produce practically indistinguishable δ(COOH) chemical shifts with values ranging from 13.4 to 14.2 ppm. In all cases very strong hydrogen bond interactions of the carboxylic protons with the oxygen of the DMSO molecule were observed with OH···O distances of 1.59 to 1.62 Å and bond angles of 168.5° to 171.2°. These hydrogen bond distances are significantly shorter than those observed in the centro-symmetric hydrogen bond interactions through the carboxylic groups with OH···O distances of 1.66 Å.

Preprints (www.preprints.org) | NOT PEER-REVIEWED | Posted: 25 July 2023 doi:10.20944/preprints202307.1662.v1

The results of comparing the complexation energy of the caproleic dimer in Figure 6a and the caproleic acid-DMSO complex in Figure 7a are very informative. For the structure 6a, the complexation energy is -21.2 kcal/mole, while it is -18.0 kcal/mole for the 7a. Given that the centro-symmetric hydrogen bond is double while in the caproleic-DMSO complex, only one hydrogen bond is formed, DMSO seems to be the most potent antagonist for this interaction.

Similar results were obtained with the α-linolenic acid. The OH···O hydrogen bond distance (1.64 Å), the O–H···O bond angle (168.5°) and the COOH chemical shift (δ = 13.43 ppm) are indicative of a very strong intermolecular hydrogen bond with a single solvation molecule of DMSO (Table 3 and Supplementary Figure S2).

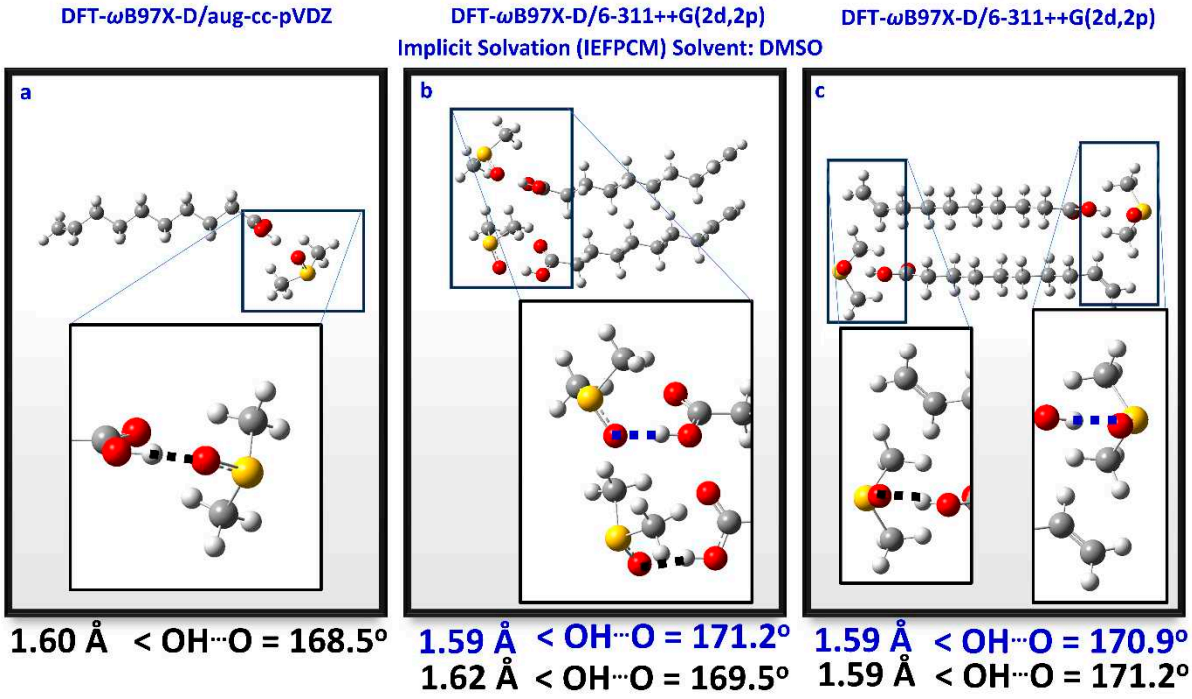

Figure 7. Optimized structures of caproleic acid (CA) with a discrete solvation molecule of DMSO on the carboxylic group: single molecule of CA (a); dimeric structures of CA in parallel (b) and antiparallel configuration (c).

Table 3. Calculated δ(COOH) chemical shifts of the free fatty acids under study with a discrete solvation molecule of DMSO.

FFA	Intermolecular interaction	δ(COO<u>H</u>) (ppm)
CA	COO-H···DMSO	13.6
CA dimer parallel	COO-H··· DMSO	14.3, 14.0, 13.7, 13.0
CA dimer antiparallel	COO-H··· DMSO	13.8, 13.8, 13.8, 13.2
ALA	COO-H··· DMSO	13.43

3. Materials and Methods

3.1. Chemicals and Reagents

Caproleic acid, purity ≥ 96%, oleic acid, purity ≥ 99% (GC), and α-linolenic acid, purity ≥ 99%, were purchased from Sigma-Aldrich. EPA, purity > 99%, and DHA, purity > 99%, were purchased from Larodan. Chloroform-d_1 and DMSO-d_6, 99.8%, were obtained from Deutero. Molecular sieves (3Å) were obtained from Sigma-Aldrich and activation was achieved by heating at 200-230°C for 24 h and the use of high vacuum for 3 h.

Preprints (www.preprints.org) | NOT PEER-REVIEWED | Posted: 25 July 2023 doi:10.20944/preprints202307.1662.v1

3.2. Variable Temperature and Concentration ^{1}H NMR Chemical Shifts and 1D ^{1}H NMR Transient NOE

Variable temperature ^{1}H NMR experiments were performed on a Bruker AVANCE NEO 500 spectrometer, controlled by the software TopSpin 3.2. The temperature was maintained and measured with an accuracy of ± 0.1°C. Chemical shifts were reported with respect to the solvent residual signal ($CDCl_3$/DMSO-d_6). Correction of temperature dependencies of the chemical shifts of the solvents was not applied since they are very small [48,49], in absolute terms, falling well below the anticipated range of $\Delta\delta/\Delta T$ values of the carboxylic protons. Variable concentration (100 to 20 mM) 1D transient NOE experiments [50–52] were performed with the use of the pulse program selnogp with pulse field gradients (PFG). The recovery delay was set to 200 μs and the shaped pulse to 50 ms [28]. NMR experiments were performed on freshly prepared solutions to avoid the formation of significant amounts of primary and secondary oxidation products [53,54].

3.3. DFT Calculations of ^{1}H NMR Chemical Shifts and Complexation Energies

All geometries were optimized at the DFT-ωB97X-D level of theory [55,56]. Three basis sets were adopted (aug-cc-pVDZ, 6-311++G(2d,2p), and 6-31+G(d,p)) adjusted at the relative molecular system size and computational cost. The selected functional is a range-separated functional, based on modified Becke's 97 functional with added dispersion corrections. It comprises 22% Hartree-Fock exchange for the short range and 100% Hartree-Fock for the long range. A standard error function with a default range separation parameter value of $\omega = 0.2$ was applied for the intermediate region. Tight optimization criteria were employed (RMS force = $1*10^{-5}$), while subsequent frequency calculations located no imaginary frequencies, confirming that the optimized structures are true minima. The GIAO (Gauge-Independent Atomic Orbital) [57] was employed to calculate the NMR spectrum. The counterpoise corrections included the basis set superposition error (BSSE) in the complexation energy calculations [58]. The Polarizable Continuum Model (PCM) with the integral equation formalism variant (IEFPCM) was employed for implicit solvation [59]. The computations were run on the FASRC Odyssey cluster supported by the FAS Division of Science Research Computing Group at Harvard University.

4. Conclusion

The combined use of variable temperature and concentration ^{1}H NMR chemical shifts of the carboxylic protons, variable concentration transient 1D NOE experiments, and DFT calculations of ^{1}H NMR chemical shifts are an effective approach to investigate a variety of low energy structures of unsaturated and polyunsaturated FFAs in chloroform and DMSO solution. More specific:

(a) Caproleic acid, oleic acid, α-linolenic acid, and EPA, in various concentrations in chloroform solution (c = 100 to 20 mM), exist mainly in the form of hydrogen-bonded dimers through carboxylic groups in an equilibrium of parallel and antiparallel interdigitated structures. The correlation times for molecular tumbling are within the extreme narrowing condition for all FFAs, therefore, the hydrogen-bonded aggregates are of low molecular weight. In DHA a structural model of an intermolecular hydrogen bond through carboxylic groups and an intermolecular hydrogen bond between the carboxylic group of one molecule and the terminal double bond of a second molecule is shown to play a role, as in the case of the liquid state [28].

(b) In DMSO solution, at low concentration c = 20 mM, all the FFAs investigated show a strong hydrogen bond interaction of a single discrete solvation molecule of DMSO with the carboxylic group, without hydrogen bonded dimers through the carboxylic groups. 1D NOE experiments and DFT calculations show the presence of parallel and antiparallel interdigitated configurations of low molecular weight within the extreme narrowing condition ($\omega_o\tau_c << 1$).

The present study shows the great conformational flexibility of mono- and polyunsaturated FFAs in various solvents and the importance of the combined use of NMR and DFT studies [18,19,27,28,60–63]. The significant conformational flexibility of FFAs was also considered to be the main reason that their location in the binding site FA7 in the human serum albumin could not be determined accurately [18,19,63] in the available X-ray structural data [64–66]. The structures of free

fatty acids and their oxidation products [53,54], in various solvents with varying hydrogen bond and solvation abilities, are currently under investigation with the combined use of NMR and DFT studies.

Supplementary Materials: The following supporting information can be downloaded at the website of this paper posted on Preprints.org. Figure S1: 1D transient NOE (500 MHz) NMR spectra of caproleic acid (CA), c = 20 mM in $CDCl_3$ solution (A) and c = 20 mM in DMSO-d_6 solution (B) (number of scans=512, T=298K, T_{acq}=4.09s, relaxation delay=4s) using various mixing times (τ_m). The excited α-CH_2 group (denoted with the asterisk (*)), is reduced by a factor of 30, relative to the amplitude of the NOE signals in the region up to 5.9 ppm. Figure S2: Optimized structure of α-linolenic acid (ALA) with a discrete solvation molecule of DMSO on the carboxylic group.

Author Contributions: Conceptualization, G.P. and I.P.G.; NMR experiments, T.V.; Computations, G.P.; Methodology, T.V., M.S., G.P. and I.P.G.; Funding acquisition and project administration, I.P.G. All authors have read and agreed to the published version of the manuscript.

Funding: The research has been co-financed by the Hellenic Foundation for Research and Innov"tion (H.F.R.I.) under the "First Call for H.F.R.I. Research Projects to support Faculty members and Researchers and the procurement of high-co"t research equipment grant" (Project Number: 2050).

Institutional Review Board Statement: Not applicable.

Data Availability Statement: Data will be made available on request.

Conflicts of Interest: The authors declare no conflict of interest.

Sample Availability: Samples of the compounds are available from the authors.

References

1. Gunstone, F.D. *Fatty acid and lipid chemistry*, 1st ed.; Springer: New York, NY, 1996.
2. Vance, D.E.; Vance, J.E. *Biochemistry of lipids, lipoproteins and membranes (new comprehensive biochemistry)*, 5th ed.; Elsevier: Amsterdam, Netherlands, 2008.
3. Akoh, C.C. Min. D.B. *Food lipids, chemistry, nutrition and biochemistry*, 2nd ed.; Marcel Dekker Inc.: New York, 2002.
4. Leray, C. *Dietary lipids for healthy brain function*, CRC Press: USA, 2021.
5. Miles, E.A.; Calder, P.C. Modulation of immune function by dietary fatty acids. *Proc. Nutr. Soc.* **1998**, *57*, 277–292. https://doi.org/10.1079/PNS19980042.
6. Oh, D.Y. Talukdar, S. Bae, E.J. Imamura, T. Morinaga, H. Fan, W. Li, P. Lu, W.J. Watkins, S.M. Olefsky, J.M. GPR120 is an omega-3 fatty acid receptor mediating potent anti-inflammatory and insulin-sensitizing effects. *Cell* **2010**, *142*, 687–698. https://doi.org/10.1016/j.cell.2010.07.041.
7. Simopoulos, A.P. The importance of the omega-6/omega-3 fatty acid ratio in cardiovascular disease and other chronic diseases. *Exp. Biol. Med.* **2008**, *233*, 674-688. https://doi.org/10.3181/0711-MR-311.
8. Gupta, R.; Lakshmy, R.; Abraham, R.A.; Reddy, K.S.; Jeemon, P.; Prabhakaran, D. Serum omega-6/omega-3 ratio and risk markers for cardiovascular disease in an industrial population of Delhi, *Food Nutr. Sci.* **2013**, *4*, 94-97. Doi: 10.4236/fns.2013.49A1015.
9. Blasbalg, T.L.; Hibbeln, J.R.; Ramsden, C.E.; Majchrzak, S.F.; Rawlings, R.R. Changes in consumption of omega-3 and omega-6 fatty acids in the United States during the 20th century, *Am. J. Clin. Nutr.* **2011**, *93*, 950-962. https://doi.org/10.3945/ajcn.110.006643.
10. Sacchi, P.; Medina, I.; Paolillo, L.; Addeo, F. High-resolution ^{13}C-NMR olefinic spectra of DHA and EPA acids, methyl esters and triacylglycerols, *Chem. Phys. Lipids* **1994**, *69*, 65-73. https://doi.org/10.1016/0009-3084(94)90028-0.
11. Aursand, M.; Grasdalen, H. Interpretation of the ^{13}C-NMR spectra of omega-3 fatty acids and lipid extracted from the white muscle of Atlantic salmon (*Salmo salar*), *Chem. Phys. Lipids* **1992**, *62*, 239-251. https://doi.org/10.1016/0009-3084(92)90061-S.
12. Gunstone, F.D.; Seth, S.; Wolff, R.L. The distribution of Δ5 polyene acids in some pine seed oils between the α- and β-chains by ^{13}C-NMR spectroscopy**,** *Chem. Phys. Lipids* **1995**, *78*, 89-96. https://doi.org/10.1016/0009-3084(95)02488-5.
13. Gunstone, F.D.; Seth, S. A study of the distribution of eicosapentaenoic acid and docosahexaenoic acid between the α and β glycerol chains in fish oils by ^{13}C-NMR spectroscopy, *Chem. Phys. Lipids* **1994**, *72*, 119-126. https://doi.org/10.1016/0009-3084(94)90095-7.
14. Alexandri, E.; Ahmed, R.; Sidiqui, H.; Choudhary, M.I.; Tsiafoulis, C.G.; Gerothanassis, I.P. High resolution NMR spectroscopy as a structural and analytical tool of unsaturated lipids in solution, *Molecules*, **2017**, *22*, 1663. https://doi.org/10.3390/molecules22101663.

15. Applegate, K.R.; Glomset, J.A. Computer-based modeling of the conformation and packing properties of docosahexanoic acid, *J. Lipid Res.* **1986**, *27*, 658-680. https://doi.org/10.1016/S0022-2275(20)38805-2.
16. Smith, P.; Lorenz, C.D. LiPyphylic: A python toolkit for the analysis of lipid membrane simulations, *J. Chem. Theory Comput.* **2021**, *17*, 5907-5919. https://doi.org/10.1021/acs.jctc.1c00447.
17. Manna, M.; Nieminen, T.; Vattulainen, I. Understanding the role of lipids in signaling through atomistic and multiscale simulations of cell membranes, *Annu. Rev. Biophys.* **2019**, *48*, 421-439. https://doi.org/10.1146/annurev-biophys-052118-115553.
18. Alexandri, E.; Primikyri, A.; Papamokos, G.; Venianakis, T.; Gkalpinos, V.G.; Tzakos, A.G.; Karydis-Messinis, A.; Moschovas, D.; Avgeropoulos A.; Gerothanassis, I.P. NMR and computational studies reveal novel aspects in molecular recognition of unsaturated fatty acids with non-labeled serum albumin, *FEBS J.* **2022**, *289*, 5617-5636. https://doi.org/10.1111/febs.16453.
19. Alexandri, E.; Venianakis, T.; Primikyri, A.; Papamokos, G.; Gerothanassis, I.P. Molecular basis for the selectivity of DHA and EPA in Sudlow's drug binding sites in human serum albumin with the combined use of NMR and docking calculations, *Molecules* **2023**, *28*, 3724. https://doi.org/10.3390/molecules28093724.
20. Eldho, N.V.; Feller, S.E.; Tristram-Nagle, S.; Polozov, I.V.; Gawrisch, K. Polyunsaturated docosahexaenoic vs docosapentaenoic acids differences in lipid matrix properties from the loss of one double bond, *J. Am. Chem. Soc.* **2003**, *125*, 6409 - 6421. https://doi.org/10.1021/ja029029o.
21. Law, J.M.S.; Szori, M.; Izsak, R.; Pekne, B.; Csizmadia, I.G.; Viskolcz, B. Folded and unfolded conformations of the ω-3 polyunsaturated fatty acid family: $CH_3CH_2[CH{=}CHCH_2]_B[CH_2]_MCOOH$. First principles study, *J. Phys. Chem. A* **2006**, *110*, 6100-6111. https://doi.org/10.1021/jp058215o.
22. Iwahashi, M.; Kasahara, Y.; Matsuzawa, H.; Yagi, K.; Nomura, K.; Terauchi, H.; Ozaki, Y.; Susuki, M. Self-diffusion, dynamical molecular conformation and liquid structures of n-saturated and unsaturated fatty acids, *J. Phys. Chem. B* **2000**, *104*, 6186-6194. https://doi.org/10.1021/jp000610l.
23. Iwahashi, M.; Kasahara, Y. Dynamic molecular movements and aggregation structures of lipids in a liquid state, *Curr. Opin. Colloid Interface Sci.* **2011**, *16*, 359-366. https://doi.org/10.1016/j.cocis.2011.06.005.
24. Broadhurst, C.L.; Schmidt, W.F.; Nguyen, J.K.; Qin, J.; Chao, K.; Aubuchon, S.R.; Kim, M.S. Continuous gradient temperature Raman spectroscopy and differential scanning calorimetry of N-3DPA and DHA from -100 to 10°C, *Chem. Phys. Lipids* **2017**, *204*, 94-104. https://doi.org/10.1016/j.chemphyslip.2017.03.002.
25. Schmidt, W.F.; Chen. F.; Broadhurst, C.L.; Nguyen, J.K.; Qin, J.; Chao, K.; Kim, M.S. GTRS and 2D-NMR studies of alpha and gamma linolenic acids each containing the same H_2C14-(H–C=C–H)–$C11H_2$–(H–C=C–H)–$C8H_2$ moiety, *J. Mol. Struct.* **2019**, *1196*, 258-270. https://doi.org/10.1016/j.molstruc.2019.06.046.
26. Bagheri Novir, S.; Tirandaz, A.; Lotfipour, H. Quantum study of DHA, DPA and EPA anticancer fatty acids for microscopic explanation of their biological functions, *J. Mol. Liq.* **2021**, *325*, 114646. https://doi.org/10.1016/j.molliq.2020.114646.
27. Venianakis, T.; Primikyri, A.; Alexandri, E.; Papamokos, G.; Gerothanassis, I.P. Molecular models of three ω-3 fatty acids based on NMR and DFT calculations of ^{1}H NMR chemical shifts, *J. Mol. Liq.* **2021**, *342*, 117460. https://doi.org/10.1016/j.molliq.2021.117460.
28. Venianakis, T.; Siskos, M.; Papamokos, G.; Gerothanassis, I.P. NMR and DFT studies of monounsaturated and ω-3 polyunsaturated free fatty acids in the liquid state reveal a novel atomistic structural model of DHA, *J. Mol. Liq.* **2023**, *376*, 121459. https://doi.org/10.1016/j.molliq.2023.121459.
29. Neratzaki, A.A.; Tsiafoulis, C.G.; Charisiadis, P.; Kontogianni, V.G.; Gerothanassis, I.P. Novel determination of the total phenolic contents in crude plant extracts by the use of ^{1}H NMR of the –OH spectral region, *Anal. Chim. Acta* **2011**, *688*, 54-60. https://doi.org/10.1016/j.aca.2010.12.027.
30. Siskos, M.G.; Tzakos, A.G.; Gerothanassis, I.P. Accurate ab initio calculations of O–H···O and O–H···-O proton chemical shifts: towards elucidation of the nature of the hydrogen bond and prediction of hydrogen bond distances, *Org. Biomol. Chem.* **2015**, *13*, 8852-8868. https://doi.org/10.1039/C5OB00920K.
31. Siskos, M.G.; Iqbal Choudhary, M.; Gerothanassis, I.P. Hydrogen atomic positions of O–H···O hydrogen bonds in solution and in the solid state: the synergy of quantum chemical calculations with ^{1}H-NMR chemical shifts and X-ray diffraction methods, *Molecules* **2017**, *22(3)*, 415. https://doi.org/10.3390/molecules22030415.
32. Yamamoto, S.; Matsuda, H.; Kasahara, Y.; Iwahashi, M.; Takagi, T.; Bada, T.; Kanamori, T. Dynamic molecular behavior of semi-fluorinated oleic, elaidic and stearic acids in the liquid state, *J. Oleo Sci.* **2012**, *61*, 649-657. https://www.jstage.jst.go.jp/article/jos/61/11/61_649/_pdf.
33. Goldman, M.A.; Emerson, M.T. Hydrogen-bonded species of acetic acid in inert solvents, *J. Phys. Chem.* **1973**, *77*, 2295-2299. https://doi.org/10.1021/j100638a008.
34. Marechal, Y. H-bonded open and cyclic dimers in the gas phase, *J. Mol. Struct.* **1988**, *189*, 55-63. https://doi.org/10.1016/0022-2860(88)80212-6.
35. Tjahjono, M.; Cheng, S.; Li, C.; Garland, M. Self-association of acetic acid in dilute deuterated chloroform. wide-range spectral reconstructions and analysis using FTIR spectroscopy, BTEM, and DFT, *J. Phys. Chem. A* **2010**, *114*, 12168-12175. https://doi.org/10.1021/jp106720v.

36. Nagy, P.I. Competing intramolecular vs. intermolecular hydrogen bonds in solution, *Int. J. Mol. Sci.* **2014**, *15(11)*, 19562-19633. https://doi.org/10.3390/ijms151119562.
37. Issaoui, N.; Ghalla, H.; Brandan, S.A.; Bardak, F.; Flakus, H.I.; Atac, A.; Oujia, B. Experimental FTIR and FT-Raman and theoretical studies on the molecular structures of monomer and dimer of 3-thiopheneacrylic acid, *J. Mol. Struct.* **2017**, *1135*, 209-221. https://doi.org/10.1016/j.molstruc.2017.01.074.
38. Lengvinaitė, D.; Aidas, K.; Kimtys, L. Molecular aggregation in liquid acetic acid: insight from molecular dynamics/quantum mechanics modelling of structural and NMR properties, *Phys. Chem. Chem. Phys.* **2019**, *21(27)*, 14811-14820. https://doi.org/10.1039/C9CP01892A.
39. Jozwiak, K.; Jezierska, A.; Panek, J.J.; Goremychkin, E.A.; Tolstoy, P.M.; Shenderovich, I.G.; Filarowski, A. Inter- vs. intramolecular hydrogen bond patterns and proton dynamics in nitrophthalic acid associates, *Molecules* **2020**, *25*, 4720. https://doi.org/10.3390/molecules25204720.
40. Ernst, J.; Sheldrick, W.S.; Fuhrhop, J.-H. The structures of the essential unsaturated fatty acids. Crystal structures of linoleic and evidence for the crystal structures of α-linolenic acid and arachidonic acid, *Z. Naturforsch.* **1979**, *34b*, 706-711. https://doi.org/10.1515/znb-1979-0512.
41. Iwahashi, M.; Kasahara, Y.; Minami, H.; Matsazawa, H.; Susuki, M.; Ozaki, Y. Molecular behaviors of n-fatty acids in liquid state, *J. Oleo Sci.* **2002**, *51*, 157-164. https://doi.org/10.5650/jos.51.157.
42. Takahashi, O.; Kohno, Y.; Nishio, M. Relevance of weak hydrogen bonds in the conformation of organic compounds and bioconjugates: evidence from recent experimental data and high-level ab initio MO calculations, *Chem. Rev.* **2010**, *110(10)*, 6049-6076. https://doi.org/10.1021/cr100072x.
43. Maier, J.M.; Li, P.; Vik, E.C.; Yehl, C.J.; Strickland, S.M.S.; Shimizu, K.D. Measurement of solvent OH-pi interactions using a molecular balance, *J. Am. Chem. Soc.* **2017**, *139(19)*, 6550-6553. https://doi.org/10.1021/jacs.7b02349.
44. Kalra, K.; Gorle, S.; Cavallo, L.; Oliva, R.; Chawla, M. Occurrence and stability of lone pair-pi and OH-pi interactions between water and nucleobases in functional RNAs, *Nucleic Acids Res.* **2020**, *48(11)*, 5825-5838. https://doi.org/10.1093/nar/gkaa345.
45. Oku, K.; Watanabe, H.; Kubota, M.; Fukuda, S.; Kurimoto, M.; Tsujisaka, Y.; Komori, M.; Inoue, Y.; Sakurai, M. NMR and quantum chemical study on the OH···π and CH···O interactions between trehalose and unsaturated fatty acids: implication for the mechanism of antioxidant function of trehalose, *J. Am. Chem. Soc* **2003**, *125(42)*, 12739-12748. https://doi.org/10.1021/ja034777e.
46. Wudarczyk, J.; Papamokos, G.; Marszalek, T.; Nevolianis, T.; Schollmeyer, D.; Pisula, W.; Floudas, G.; Baumgarten, M.; Mullen, K. Dicyanobenzothiadiazole derivatives possessing switchable dielectric permittivities, *ACS Appl. Mater. Interf.* **2017**, *9*, 20527-20535. https://doi.org/10.1021/acsami.7b03060.
47. Pashkovskaya, A.A.; Vazdar, M.; Zimmermann, L.; Jovanovic, O.; Pohl, P.; Pohl, E.E. Mechanism of long-chain free fatty acid protonation at the membrane-water interface, *Biophys. J.* **2018**, *114*, 2142-2151. https://doi.org/10.1016/j.bpj.2018.04.011.
48. Cross, B.P.; Schleich, T. Temperature dependence of the chemical shifts of commonly employed proton n.m.r. reference compounds, *Org. Magn. Reson.* **1977**, *10*, 82-85. https://doi.org/10.1002/mrc.1270100121.
49. Hoffman, R.E. Standardization of chemical shifts of TMS and solvent signals in NMR solvents, *Magn. Reson. Chem.* **2006**, *44*, 606-616. DOI: 10.1002/mrc.1801.
50. Kessler, H.; Oschkinat, H.; Griesinger, C.; Bermel, W. Transformation of homonuclear two-dimensional NMR techniques into one-dimensional techniques using Gaussian pulses, *J. Magn. Reason.* **1986**, *70*, 106-133. https://doi.org/10.1016/0022-2364(86)90366-5.
51. Stott, K.; Stonehouse, J.; Keeler, J.; Hwang, T.-L.; Shaka, A. J. Excitation sculpting in high-resolution nuclear magnetic resonance spectroscopy: Application to selective NOE experiments, *J. Am. Chem. Soc.* **1995**, *117*, 4199-4200. https://doi.org/10.1021/ja00119a048.
52. Neuhaus, D.; Williamson, P.M. *The nuclear Overhauser effect in structural and conformational analysis*, VHC Publishers, New York, NY, 1989.
53. Kontogianni, V.G.; Gerothanassis, I.P. Analytical and structural tools of lipid hydroperoxides: Present state and future perspectives, *Molecules* **2022**, *27*, 2139. https://doi.org/10.3390/molecules27072139.
54. Ahmed, R.; Siskos, M.G.; Siddiqui, H.; Gerothanassis, I.P. DFT calculations of $\delta(^{13}C)$ and (^{1}H) chemical shifts and $^{3}J(^{13}C\text{-}O\text{-}O\text{-}^{1}H)$ coupling constants as structural and analytical tools in hydroperoxides: prospects and limitations of $^{1}H\text{-}^{13}C$ HMBC experiments, *Magn. Reson. Chem.* **2022**, *60*, 970-984. https://doi.org/10.1002/mrc.5298.
55. Chai, J.D.; Head-Gordon, M. Systematic optimization of long-range corrected hybrid density functionals, *J. Chem. Phys.* **2008**, *128*, 084106. https://doi.org/10.1063/1.2834918.
56. Chai, J.D.; Head-Gordon, M. Long-range corrected hybrid density functionals with damped atom–atom dispersion corrections, *Phys. Chem. Chem. Phys.* **2008**, *10*, 6615-6620. https://doi.org/10.1039/B810189B.
57. Cheeseman, J.R.; Trucks, G.W.; Keith, T.A.; Frisch, M.J. A Comparison of models for calculating nuclear magnetic resonance shielding tensors, *J. Chem. Phys.* **1996**, *104*, 5497-5509. https://doi.org/10.1063/1.471789.

58. Boys, S.F.; Bernardi, F. The calculation of small molecular interactions by the differences of separate total energies. Some procedures with reduced errors, *Mol. Phys.* **1970**, *19*, 553-566. https://doi.org/10.1080/00268977000101561.
59. Tomasi, J.; Mennucci, B.; Cammi, R. Quantum mechanical continuum solvation models, *Chem. Rev.* **2005**, *105*, 2999-3094. https://doi.org/10.1021/cr9904009.
60. Bursch, M.; Mewes, J.-M.; Hansen, A.; Grimme, S. Best-practice DFT protocols for basic molecular computational chemistry, *Angew. Chem. Int. Ed.* **2022**, *61(42)*, e202205735. DOI: https://doi.org/10.1002/anie.202205735.
61. Papamokos, G.; Dimitriadis, T.; Bikiaris, D.N.; Papageorgiou, G.Z.; Floudas, G. Chain conformation, molecular dynamics, and thermal properties of poly(n-methylene 2,5-furanoates) as a function of methylene unit sequence length, *Macromolecules* **2019**, *52(17)*, 6533-6546. https://doi.org/10.1021/acs.macromol.9b01320.
62. Gerothanassis, I.P. Ligand-observed in-tube NMR in natural products research: A review on enzymatic biotransformations, protein–ligand interactions, and in-cell NMR spectroscopy, *Arab. J. Chem.* **2023**, *16*, 104536. https://doi.org/10.1016/j.arabjc.2022.104536
63. Primikyri, A.; Papamokos, G.; Venianakis, T.; Sakka, M.; Kontogianni, V.; Gerothanassis, I.P. Structural basis of artemisinin binding sites in serum albumin with the combined use of nmr and docking calculations, *Molecules* **2022**, *27*, 5912. https://doi.org/10.3390/molecules27185912.
64. Bhattacharya, A.A.; Grüne, T.; Curry, S. Crystallographic analysis reveals common modes of binding of medium and long-chain fatty acids to human serum albumin, *J. Mol. Biol.* **2000**, *303*, 721–732. https://doi.org/10.1006/jmbi.2000.415.
65. Petitpas, I.; Grüne, T.; Bhattacharya, A.A.; Curry, S. Crystal structures of human serum albumin complexed with monounsaturated and polyunsaturated fatty acids, *J. Mol. Biol.* **2001**, *314(5)*, 955–960. https://doi.org/10.1006/jmbi.2000.5208.
66. Ghuman, J.; Zunszain, P.A.; Petitpas, I.; Bhattacharya, A.A.; Otagiri, M.; Curry, S. Structural basis of the drug-binding specificity of human serum albumin, *J. Mol. Biol.* **2005**, *353*, 38-52. https://doi.org/10.1016/j.jmb.2005.07.075.